EPJ Web of Conferences **68**, 00034 (2014)
DOI: 10.1051/epjconf/20146800034
© Owned by the authors, published by EDP Sciences, 2014

# A New Approach for Debonding Characterization

Fergyanto E. Gunawan[a]

Binus Graduate Programs, Bina Nusantara University, Jakarta 11480, Indonesia

**Abstract.** Debonding or decohesion along a fiber-matrix interface frequently becomes the main mode of failure of a composite structure. Hence, a methodology to evaluate the decohesion is of interest of many scientists and engineers. Unfortunately, many existing methods such as the micro-bond method, the fiber pull-out method, and the fiber push-out method are too restrictive in term of the specimen design and the rate of loading. In this work, we propose a methodology to characterize the decohesion at various loading rates and verify the method experimentally.

## 1 Introduction

Composite materials are extremely important in development of many recent technologies that require engineering materials having very high the strength-to-weight ratio. For an example, each Boeing 787 contains approximately 35 tons of carbon fiber reinforced plastic [1]. Traditionally, damages and failures in composite materials are harder to model in comparison to those in conventional materials. However, during the last few years, we witnessed that the energy-based approach particularly using the cohesive zone model seems to provide a reasonable prediction particularly for delamination and debonding [2–5]. This numerical approach is pervasive than that of the analytical approach [6].

Three methods are widely used to quantify the debonding. Those methods are the micro-bond method [7–10], the fiber pull-out method [11–14], and the fiber push-out method [15–18]. However, each of those existing methods is often only suitable for a specific mode and rate of loading. The micro bond method is only suitable when the applied load is static. The push-out test method can be used for static and dynamic loads; however, a major adjustment has to be made particularly in the specimen design when the applied load is dynamic.

In this article, we extend our earlier methodology [3], which was designed for the dynamic load, to the case of the static load, and compare the results of the both cases.

## 2 Research Methodology

The debonding is a phenomenon on a microscopic scale; therefore, it is difficult to quantify directly. The existing methods usually combine an experimental approach and a numerical approach. The earlier approach is performed to record structural responses and to observe debonding phenomenon, and the later approach is performed to quantify the debonding-related parameters. The same approach will be adopted in the present work.

## 3 Modeling and Experiment

### 3.1 Debonding Specimen

The proposed specimen for the static and dynamic debonding tests is shown in Figure 1. It has the following geometry: the specimen nominal diameter ($d$) = 9.5 mm, the diameter of the bundled fiber ($d_f$) = 1 mm and 2 mm, the notch depth ($c$) = 3 mm, and the gage location ($b$) was 20 mm from the notch. For the static test, the specimen length ($L$) was 72 mm, and the notch was located in the middle. Meanwhile, for the dynamic test, the length was 200 mm, and the notch ($L_n$) was located at 90 mm.

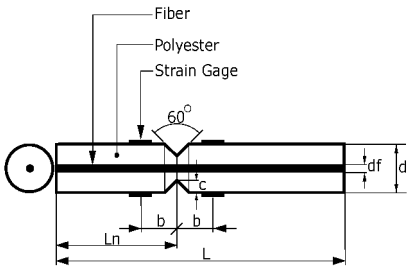


**Fig. 1.** Geometry of the cylindrical-type specimen

### 3.2 Experimental Apparatus

In the static test, the specimen was placed in the holder depicted in Fig. 2, and then pulled with a tension test machine until the debonding took place on the fiber-matrix interface. Three data were recorded: the applied load, the debonding length, and the specimen displacement.

[a] Corresponding author: fgunawan@binus.edu and f.e.gunawan@gmail.com

This is an Open Access article distributed under the terms of the Creative Commons Attribution License 2.0, which permits unrestricted use, distribution, and reproduction in any medium, provided the original work is properly cited.

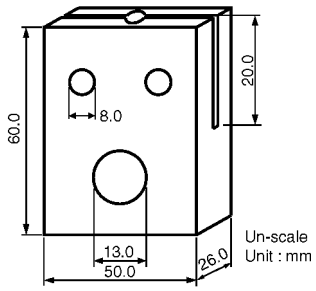


**Fig. 2.** The specimen holder for the static test

In the dynamic test, the specimen was placed in a Hopkinson bar test apparatus as shown in Fig. 3. In this test, the stress pulse was generated by striking the load transfer rod with the steel ball. The load transfer road was made of steel with a length of 1 m and a diameter of 20 mm. Prior the test, four strain gages were mounted to each specimen, and the impact-site of the specimen was attached to the end of the load transfer rod. The gage was connected to a Wheatstone bridge in a half-bridge configuration; hence, the strains due to the bending wave, if any, could be canceled out. The data from the bridge were recorded in a computer via a TDS-700 transient converter and a CDV/CDA-700A signal conditioner. The transient converter could sample the data at a rate of 0.1 μs.

From the both tests, the debonding on the specimens was usually visible with a naked eye (for an example, see Fig. 4)

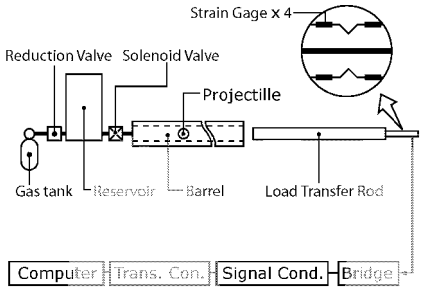


**Fig. 3.** The schematic diagram of the air gun impact system

**Fig. 4.** The debonding in the fiber-matrix interface of a specimen.

### 3.3 Modeling

Debonding is often difficult to be characterized directly from experimental measured data. An indirect approach is more common and was adopted in the this work. The approach was based on the the finite element method with a cohesive zone model to model the decohesion. The parameters associated with the cohesive zone model were established iteratively such that the numerical model produced a response similar to those observed in the experiments in microscopic and macroscopic scales.

#### *3.3.1 Bilinear Traction-Separation Model*

The cohesive constitutive model, or the traction-separation model [19], that relates the traction T to the separation $\Delta$ at the interface, was that governed by a bilinear softening model [20]. The both traction and separation have two components:

$$\mathrm{T} = \begin{pmatrix} T_n & T_s \end{pmatrix}^T, \text{ and } \Delta = \begin{pmatrix} \Delta_n & \Delta_s \end{pmatrix}^T, \tag{1}$$

where the subscript $n$ denoted the normal direction and $s$ denoted the shear or tangential direction. The superscript $c$ denoted the critical value, which was a material constant. Therefore, $T_n^c$ and $T_s^c$ denoted the interface normal strength and shear strength, respectively. The symbol $\Delta_c$ denoted the displacement when a complete separation occurred.

In this paper, the cohesive model was implemented on zero thickness elements; therefore, the nominal strains could be defined as

$$\varepsilon_n = \Delta_n, \text{ and } \varepsilon_s = \Delta_s. \tag{2}$$

The elastic part of the traction-separation model could then be written as

$$\mathrm{T} = \begin{pmatrix} T_n \\ T_n \end{pmatrix} = \begin{bmatrix} E_n & 0 \\ 0 & E_s \end{bmatrix} \begin{pmatrix} \varepsilon_n \\ \varepsilon_s \end{pmatrix} = \mathrm{E}\varepsilon, \tag{3}$$

where the normal and shear deformations were uncoupled. The symbols $E_n$ and $E_s$ denoted the elastic moduli for the normal and shear modes, respectively.

In the current approach, the debonding was assumed to initiate when a quadratic interaction involving the nominal stress ratios reached one, or mathematically speaking:

$$\left( \frac{\langle T_n \rangle}{T_n^c} \right)^2 + \left( \frac{\langle T_s \rangle}{T_s^c} \right)^2 = 1, \tag{4}$$

where $\langle \cdot \rangle$ was the Macaulay brackets that set any negative values to zero. Hence, a pure compression deformation or stress state did not initiate debonding. However, when the debonding had initiated by an amount of $D$, where $0 \le D \le 1$, the material strengths degraded:

$$T_n = \begin{cases} (1-D)\overline{T}_n, \overline{T}_n \ge 0 \\ \overline{T}_n, \text{otherwise} \end{cases} \tag{5}$$

for the normal traction, and

$$T_s = (1-D)\overline{T}_s \tag{6}$$

for the shear traction. The symbols $\overline{T}_n$ and $\overline{T}_s$ were the stress components predicted by the elastic traction-separation behavior for the current strains without debonding.

The debonding variable D was computed by

$$D = \frac{\Delta^c_{\text{mix}}(\Delta^{\max}_{\text{mix}} - \Delta^0_{\text{mix}})}{\Delta^{\max}_{\text{mix}}(\Delta^c_{\text{mix}} - \Delta^0_{\text{mix}})} \tag{7}$$

where those mix mode displacements were computed by

$$\Delta_{\text{mix}} = \sqrt{\langle \Delta_n \rangle^2 + \Delta_s{}^2} \,. \tag{8}$$

In Eq. (7), the $\Delta^0_{\text{mix}}$ denoted the displacement at the onset of damage, and the $\Delta^c_{\text{mix}}$ denoted the displacement when complete separation had occurred. The both $\Delta^0_{\text{mix}}$ and $\Delta^c_{\text{mix}}$ could easily be derived from the cohesive model parameters of the elastic modulus, the critical cohesive strength, and the critical cohesive energy. The $\Delta^{\max}_{\text{mix}}$ referred as the maximum value of the effective displacement attained during the loading history.

Therefore, after the onset of debonding $\Delta^0$, the interface strengths in both the normal and shear modes gradually would decrease to zero. The area under the traction-separation curve was the critical cohesive energies, $G^c_n$ and $G^c_s$:

$$\int_0^{\Delta_n} T_n(\Delta_n) d\Delta_n = G^c_n \,, \tag{9}$$

for the normal mode, and

$$\int_0^{\Delta_s} T_s(\Delta_s) d\Delta_s = G^c_s \,, \tag{10}$$

for the shear mode. The critical cohesive energy on the mix mode could be defined based on a power law fracture criterion:

$$\left(\frac{G_n}{G^c_n}\right)^{\alpha} + \left(\frac{G_s}{G^c_s}\right)^{\alpha} = 1 \,. \tag{11}$$

The power law criterion with $\alpha = 1$ was found to be suited to predict failure of thermoplastic matrix composites [21].

### *3.3.2 The Finite Element Models and Fracture Parameters*

The finite element method was used to establish a mechanical model that relates a macroscopic parameter recorded in the experiment—such as the maximum strain or the applied load—to the microscopic parameter, that is the debonding length. The related finite element meshes, for the static case and dynamic case, are reproduced in Fig. 5 and Fig. 6. Those models were symmetric with respect to their longitudinal axis.

To anticipate occurrence of the debonding and matrix fracture, zero thickness cohesive elements were implemented along the lines denoted by matrix interface and fiber-matrix interface in those figures. The cohesive elements in the matrix-matrix interface were employed to anticipate the matrix fracture; and in the meantime, the same type of elements in the fiber-matrix interface was for the debonding. Clearly, this approach assumed the fracture process zone occurred along a prescribed line.

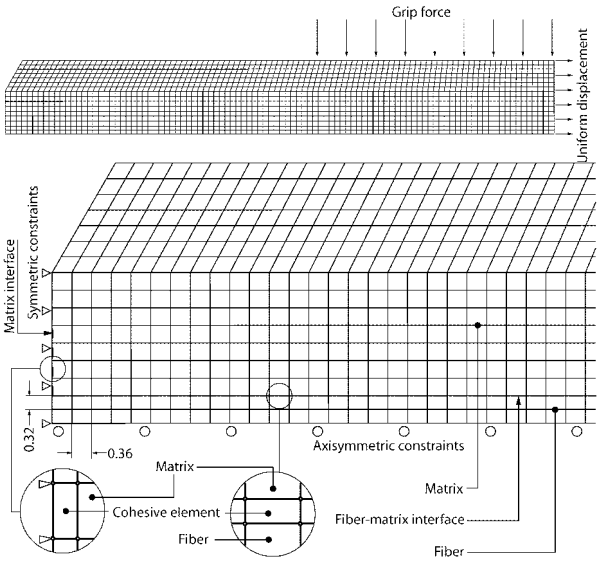


**Fig. 5.** Finite element model mesh for the static case.

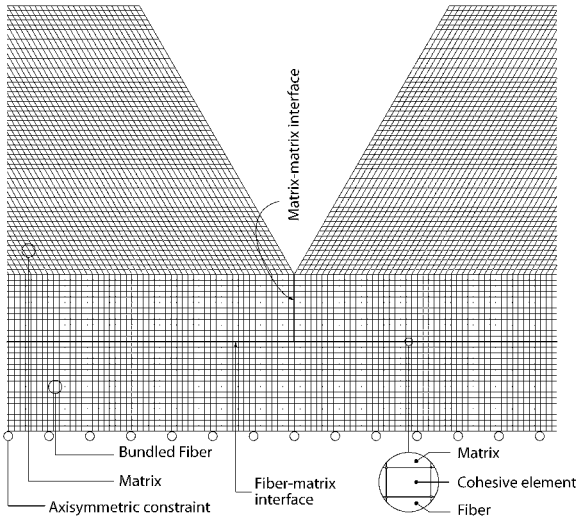


**Fig. 6.** Finite element model mesh for the dynamic case.

The identification of the cohesive zone model's parameters—the strength and the critical cohesive energy—was performed in two steps. We established those parameters for the matrix-matrix interface firstly, and then, for the fiber-matrix interface. The identification was an iterative process until the numerical model produced a response comparable to that observed in the experiment (see Fig. 7 for the static case and Fig. 8 for the dynamic case.). The identification provided the parameters of the cohesive zone model as presented in Table 1.

**Table 1**. The parameters of the cohesive zone model for the static and dynamic cases

| | Normal Mode | | Shear Model | |
|---|---|---|---|---|
| | $T_n^c$ (MPa) | $G_n^c$ (MPa· mm) | $T_s^c$ (MPa) | $G_s^c$ (MPa· mm) |
| Static | 15 | 1.0 | 15 | 1.0 |
| Dynamic | 54 | 2.0 | 67 | 2.0 |

### 3.4 Results

The results of this study are concisely summarized in Table 1 that the dynamic strength is higher than the static strength by a factor of 3–4; meanwhile, the dynamic fracture energy is about twice higher than the static fracture energy. The idea that the material strength and fracture energy is higher in the high loading rate is traditional and acceptable. Concrete dynamic strength, for an example, would increase by 30%–50% when the loading rate was varied from 1.5 to 3 $s^{-1}$ [22]. In addition, Kalthoff and Wrinkler [23] shown, as cited by Nishioka and Atluri [24], that the fracture toughness of Araldite B double-cantilever-beam specimen increased from 0.7 MPa·$mm^{1/2}$ at the static test to 1.4 MPa·$mm^{1/2}$ at the dynamic test with a crack speed of 300 m/s. Thus, these results in Table 1 seem to be reasonable.

In regard to the debonding length prediction, the model was only capable estimating the debonding at a reasonable length that was longer than about 7.5 mm for the statically loaded case. However, when the load was dynamic, the smallest debonding was estimated at 2 mm length. These limitations were not affected by the mesh size as was indicated by a mesh sensitivity study.

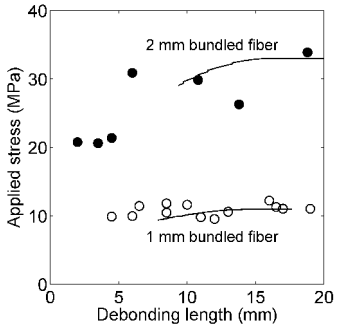


**Fig. 7.** The debonding length versus the applied stress for 1 mm and 2 mm bundled fibers. The solid line is a result of the finite element analysis, and the circle mark is a static-test result.

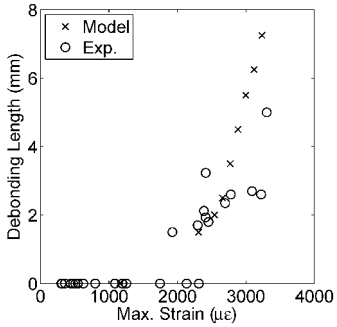


**Fig. 8.** The debonding length versus the maximum recorded strain for 1 mm bundled fiber. The cross mark is a result of the finite element analysis, and the circle mark is the dynamic-test result.

## 4 Conclusions

We have demonstrated that the cohesive zone model is capable to provide a reasonable prediction of the decohesion along a fiber-matrix interface when the specimen is subjected by a static load and a pulse-type load. It may be attractive to conclude that the model can also predict the decohesion under a moderate rate of loading; however, experimental data are clearly necessary, and such an experiment is feasible with the current proposal.

## References

1. Wikipedia, Boeing 787 dreamliner, https://en.wikipedia.org/wiki/Boeing_787_Dreamliner#Composite_materials, downloaded on June 17 (2013).
2. C. Shet and N. Chandra, Transactions of the ASME: Journal of engineering materials and technology **124**, 440 (2002)
3. Fergyanto E Gunawan, Engineering Fracture Mechanics **78**, 2731 (2011) http://dx.doi.org/10.1016/j.engfracmech.2011.07.008
4. MA Minnicino and MH Santare, Composites science and technology **72**, 2024 (2012)
5. KN Anyfantis and NG Tsouvalis, Composite structures **96**, 858 (2013)
6. E. Nwankwo, AS Fallah, and LA Louca, Journal of Sound and Vibration **332**, 1834 (2013)
7. T Schuller, W Becker, and B Lauke, The Journal of adhesion **70**, 33 (1999)
8. LP Hann, and DE Hirt, Composite Science and Technology **54**, 423 (1995)
9. B Miller, P Muri, and L Rebenfeld, Composite science and technology **28**, 17 (1987)
10. CH Liu, and JA Naim, International journal of adhesion and adhesives **1**, 311 (1981)
11. JP Favre and MC Merienne, International journal of adhesion and adhesives **1**, 311 (1981)
12. JK Kim, C Baillie, and YW Mai, Journal of material science **27**, 3143 (1991)
13. JK Wells, and PWR Beaumont, Journal of material science **20**, 1275 (1985)
14. JA Nairn, CH Liu, DA Mendels, S. Zhandarov, Fracture mechanics analysis of the single-fiber pullout test and the microbon test including the effect of friction and thermal stresses, in: Proceeding 16th annual technology conference of the American society of composites (2001)
15. LM Zhou, YW Mai, and L Ye, Composite engineering **5**, 1199 (1995)
16. G Lin, PH Geubelle, and NR Sottos, International journal of solid and structures **38**, 8547 (2001)
17. Z Li, X Bi, J Lambros, PH Geubelle, Experimental mechanics **42**, 417 (2002)
18. X Bi, Z Li, PH Geubelle, and J Lambros, Mechanics of materials **34**, 433 (2002)
19. Abaqus, ABAQUS Analysis User's Manual Version 6.8 (2008)

20. PH Geubelle, and J Baylor, Composites, Part B **29B**, 589 (1998)
21. PP Camanho, and CG Davila, Mixed-mode decohesion finite elements for the simulation of delamination in composite materials, Tech. Rep. NASA/TM-2002-211737, NASA Langley Research Center, Hampton, VA 23681-2199 (June 2002).
22. D Zheng, Q Li, Frontier architecture civil engineering of China **2**, 329 (2008)
23. JF Kalthoff, J Beinert, and S Wrinkler, Measurement of dynamic stress intensity factors for fast running and arresting cracks in double-cantilever-beam specimens, in: Fast Fracture and Crack Arrest ASTM STP 627, ASTM, 1977, pp. 161–176.
24. T Nishioka, SN Atluri, Engineering fracture mechanics **18**, 23 (1983)